1987

Spatial resolution and measurement of turbulence in the viscous sublayer using subminiature hot-wire probes

Ligrani, P.M.; Bradshaw, P.

Springer-Verlag

Ligrani, P. M., and P. Bradshaw. "Spatial resolution and measurement of turbulence in the viscous sublayer using subminiature hot-wire probes." Experiments in Fluids 5.6 (1987): 407-417.
http://hdl.handle.net/10945/62150

Experiments in Fluids 5, 407–417 (1987)

Experiments in Fluids

Spatial resolution and measurement of turbulence in the viscous sublayer using subminiature hot-wire probes

P. M. Ligrani

Department of Mechanical Engineering, 69Li, Naval Postgraduate School, Monterey, CA 93943-5000, USA

P. Bradshaw

Department of Aeronautics, Imperial College of Science and Technology, Prince Consort Road, London SW7 2BY, Great Britain

Abstract. Measurements in the viscous sublayer of a flat-plate turbulent boundary layer in air, using single hot-wire sensors with lengths from 1–60 viscous length scales show that, at a given distance from the surface, the turbulence intensity, flatness factor, and skewness factor of the longitudinal velocity fluctuation are nearly independent of wire length when the latter is less than 20–25 times the viscous length scale (i.e. 20–25 "wall units"), and decrease significantly and abruptly for larger wire lengths. This conclusion is consistent with other workers' probability density functions of streak spacing: the lateral spacing of "streaks" in the viscous sublayer is 80–100 wall units on average with minimum spacing of 20–25 wall units, which implies that signals would be strongly attenuated by wires whose length exceeds 20–25 wall units. To achieve wire lengths of less than 20–25 wall units, subminiature hot wire probes like those described by Ligrani and Bradshaw (1987), having lengths as small as 150 μm, are necessary for sublayer measurements in typical laboratory wind tunnels. As well as the measurements mentioned above, dissipation spectra are presented, to show the effect of spanwise averaging on the high-frequency motions, which is necessarily more severe than the effect on overall intensities.

1 Introduction

Small-scale motions have many important roles in the overall behavior of turbulent shear layers. Dissipation of turbulent energy into heat occurs at small scales in all parts of the flow, while in the viscous sublayer of a turbulent wall layer even the energy-containing motion is small enough to be difficult to resolve with conventional measurement techniques. In particular, the ejection/sweep cycle or "bursting" phenomenon in the viscous sublayer (e.g. Kline et al. 1967; Kim et al. 1971; Smith 1984) takes place on scales which are of the order of ten times the viscous length scale ν/U_τ where U_τ is the friction velocity, and ν is the kinematic viscosity. Note that throughout this paper we use ν/U_τ as a length scale: very near the wall, the Kolmogorov length scale is $1.5-2.0\ \nu/U_\tau$.

Clearly, hot wires or other sensors used to measure small-scale turbulence must have a sensing length significantly less than the smallest wave length to be measured: in another paper (Ligrani & Bradshaw 1987) we discuss the manufacture and performance of hot wire probes with wire lengths as small as one viscous length scale in typical low-speed turbulence flows, while in the present paper we investigate the spatial resolution of these probes in the viscous sublayer, and present longitudinal velocity fluctuation measurements which are believed to be virtually free of spatial resolution effects.

Previous studies of small-scale turbulence in shear layers using hot wire techniques have included several by Willmarth's group at the University of Michigan. Kastrinakis et al. (1975) used multiple hot wires having a typical length and spacing of two to three viscous length scales to show that the root-mean-square streamwise vorticity reaches a maximum at about the same distance from the wall at which low-speed streaks begin to oscillate and become unstable ($y^+ = U_\tau y/\nu \simeq 17$ where y = normal distance from surface). Vorticity fluctuations were observed to be highly intermittent compared to velocity fluctuations, with a large kurtosis ("flatness factor") of the order of 6 throughout the shear layer. Such vorticity was believed to reside in the intense small-scale velocity gradients observed later by Willmarth and Bogar (1977). In that study, measurements were made using a miniature cross-wire having wire length and spacing of about 2.5 viscous lengths. Even these probes appear to suffer significant spatial resolution effects due to occasional motions with length scales smaller than the probe dimensions. In a later paper, Willmarth and Sharma (1984) discussed intermittently-occurring small-scale gradients of the longitudinal velocity, which they called "small scale shear layers". Their length scale was found to be of the same order as the viscous length, with velocity gradient magnitudes occasionally as large as the mean shear at the wall. These results were obtained from pairs of hot-wire sensors with length of approximately 0.3 viscous lengths, spaced about two viscous lengths apart in the y direction. The small-scale shear layers were occasional and intense, and were observed most often within the viscous sublayer.

The above studies focused on the fluid mechanics of small-scale motions, but incidentally indicated the possible severity of spatial resolution effects. Several studies have also been made of spatial resolution as such, the simplest case being the single spanwise hot-wire used to measure longitudinal velocity. Signals from such sensors represent a (weighted) transverse line average of fluid activity. The smallest eddies in any turbulent flow have length scales of the order of the Kolmorogov length scale, η, which is as small as one or two viscous lengths in the viscous sublayer. Willmarth and Bogar suggest that the velocity gradients may exist over distances as small as 0.05 η, but these seem to be very rare events. However, it certainly appears that wire lengths of two viscous lengths or less will be required for adequate resolution of sublayer turbulence at all wave numbers.

Up to about 10 years ago, investigations of the spatial resolution of hot wire probes were largely theoretical, and most were based on assumptions of local isotropy. One of the earliest of these is reported by Dryden et al. (1937). According to these authors, the ratio of measured to actual longitudinal energy is dependent on the ratio of wire length l to an integral length scale L_z, obtained from integrating the transverse correlation coefficient. Corrsin and Kovasznay (1949), and Frenkiel (1949, 1954) provide additional analysis and discussion of the Dryden et al. work. Frenkiel also considers correlation coefficients, integral scales, and microscales in his analysis. Uberoi and Kovasznay (1953) derive a relationship between the line-averaged, one-dimensional spectrum and the three-dimensional wave number spectrum. For large wire sensing lengths in isotropic turbulence, equations are also given relating one-dimensional spectra of the longitudinal velocity to "true" spectra free of the effects of finite spatial resolution. Wyngaard (1968) later extended this work using Pao's (1965) formulation for the "true" spectrum. The correction is valid only over wave number regions where small-scale motions are isotropic, and is in agreement with measurements from a curved mixing layer. Information is also given pertaining to two sensors in a crossed wire array. Wyngaard (1969, 1971) considers the spatial resolution of temperature sensors and vorticity meters. Bremhorst (1972) gives energy and spectra corrections for longitudinal velocity and shear stress, determined from correlation data. He shows that when the error in mean-square intensity is more than 5 percent, spectral errors are very severe at high wave numbers. Roberts (1973) gives a simple iteration method to correct measured one-dimensional spectra and cross-spectra in locally isotropic flow.

In more recent years, a number of investigators have studied sensor spatial resolution in the anisotropic flow very near walls where spatial resolution effects are most acute. All of these studies are based on measurements, using various types and lengths of sensors, without reliance on any particular correlation or spectral formulation. Blackwelder and Haritonidis (1983) showed that sensor spatial resolution is important in measurements of the mean bursting frequency in the wall layer. After accounting for the effects of spatial resolution, the mean bursting frequency, when scaled with ν and U_τ, was found to be constant and independent of Reynolds number, in contrast to uncorrected results from other sources. Johansson and Alfredsson (1983) provided additional confirmation of this, showing that the skewness of the time derivative of the longitudinal velocity was very sensitive to spatial averaging, because the small-scale ejection events (positive v', negative u') are attenuated more than the larger-scale sweeps (negative v', positive u'): here, u' and v' are velocity fluctuations in the longitudinal and normal directions, respectively. Derksen and Azad (1983) discuss the effects of sensor length on a variety of statistical properties in pipe flow at $y^+ = 150$, including spectral attenuation and fourth moments of spectra. Ligrani and Moffat (1986) documented the variation of longitudinal turbulence energy and spectra with normalized sensor length in the inner regions of a fully-rough turbulent boundary layer. Normalized spectra showed agreement with Wyngaard's (1968) correction curves at a Taylor microscale Reynolds number of 200 ($y^+ = 261$) where the small-scale turbulence is not too far from local isotropy.

Additional discussion and review of spatial averaging effects from pressure sensors, as well as hot-wires, is given by Smol'yakov and Tkachenko (1983).

In the present study, single hot-wire sensors, with various lengths, l, as small as 50 μm, are employed to determine the effect of transverse averaging on turbulence measurements in a zero pressure gradient boundary layer on a smooth wall. Attention is focussed on the region $y^+ < 40$ where the effects of spatial resolution are particularly acute and the motion at all scales is highly anisotropic. Assignment of one particular spectral formulation (e.g., Pao 1965) is inappropriate since correlation functions and spectra, which elucidate the effects of spatial resolution, vary significantly at different near-wall locations and Reynolds numbers. The dependence of total longitudinal energy $\overline{u'^2}$ on spatial averaging over transverse distances ranging from 1−60 viscous lengths (50 μm−3 mm) is discussed. With the exception of data given at only two $l^+ \equiv l\,U_\tau/\nu$ by Johansson and Alfredsson (1983), the dependence of $\overline{u'^2}$ on l^+ has never before been established with one consistent set of data. It is not even certain how small l^+ must be in order to measure $\overline{u'^2}$ without significant reductions due to spatial resolution effects. Thus, the present results extend other investigators' work, offering a more systematic examination of sensor spatial resolution.

Section 2 gives a description of the sensors, and Sect. 3 gives details on the measurement chain and probe calibration. Section 4 describes the experimental facilities. Section 5 gives measurement conditions. Results are

presented in Sects. 6 and 7. In Sect. 6, the effects of spatial resolution on longitudinal velocity statistical properties is addressed, while in Sect. 7, spatial resolution and dissipation spectra are considered.

2 Sensors

The subminiature hot-wire probes used in the present study, along with their development and use, are described by Ligrani and Bradshaw (1987). Details of construction are given by Ligrani (1984).

Twenty-one different sensors were employed ranging in length from 50 μm−3 mm. Sensors consisted of 90% platinum 10% rhodium wire. Three different diameters of wire were used: according to the manufacturer, 0.625 μm, 1.25 μm, and 5 μm. A schematic of the probes used for the $d = 0.625$ μm sensor is shown in Fig. 1. Here, coordinates x, y, and z refer to longitudinal, normal and transverse directions, respectively.

The end conditions of the 1.25 μm and 5.00 μm diameter sensors were similar to the subminiature $d = 0.625$ μm devices, since sensor length was controlled by adding varying amounts of copper plating near the ends of the sensor. The subminiature devices were not easily broken, and last indefinitely with moderately careful handling.

3 Experimental approach

For all of the tests of the present study, sensors were operated at constant overheat ratios between 1.2 and 1.6 using DISA (now DANTEC) 55DO1 constant-temperature anemometer circuits. After the anemometer bridge, the voltage signal was passed through an amplifier/filter unit. Here, the mean portion of the signal was removed and separately measured, and the fluctuating portion was low-pass filtered and amplified. A frequency-modulated analog tape recorder was then used to record the fluctuating signal, which was later transcribed to digital tape.

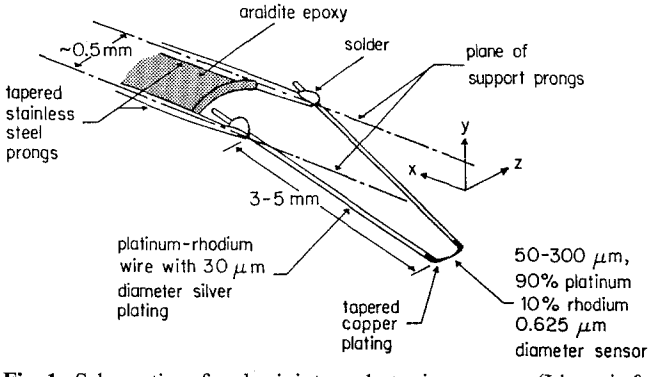

Fig. 1. Schematic of subminiature hot-wire sensor (Ligrani & Bradshaw 1987)

With previously measured mean voltages and calibration data, hot-wire voltage signals were linearized, and all statistical quantities (energy, flatness factors, skewness factors, spectra) of the instantaneous longitudinal velocity were determined using a CDC 6500 mainframe computer. Magnitudes of the rms of longitudinal velocity fluctuation, determined from the digitized voltage traces, were in agreement, within a few percent, with values determined from unlinearized rms meter measurements made of the signal leaving the anemometer bridge circuit.

Mean-flow calibration, rather than dynamic calibration, was employed. Calibrations were repeated at least twice for each set of profile points. For values of Reynolds number Re_d based on wire diameter d and mean velocity greater than 0.07, calibration data for all three wire diameters showed behavior consistent with the Collis and Williams (1959) forced convection heat transfer law. For lower Re_d, sensor heat transfer was the result of mixed convection. Here, accurate mean measurements were obtained, but the dynamic response showed discrepancies and is under further investigation. All results presented in this paper were obtained when $Re_d > 0.07$.

For all measurements presented here, the surface beneath the hot-wires was a mirror, chosen because it was flat and smooth with low thermal conductivity. The position of the probe with respect to the surface was determined using a method dependent upon linear sublayer flow properties. This was checked by using a metal wall, probe contact being indicated by closure of an electric circuit.

The smallest distance from the wall in the data which follows is 350 μm or about 560 subminiature probe diameters. Thus, no corrections for wall proximity were required, and no corrections due to the interference of the prongs with the flow were required.

For further discussion of sensor use, qualification and response, and for experimental details, the reader is referred to Ligrani and Bradshaw (1987). That paper includes additional discussion of sensor alignment, measurement uncertainty, flow blockage effects, drift, measurement chain details, signal processing details, calibration, the traversing device and measurement of probe distance from the wall, as well as details on overall subminiature sensor performance characteristics.

4 Experimental facilities

Experimental results were obtained using an Imperial College Department of Aeronautics wind tunnel described by Bradshaw (1972). It has a two-dimensional 9:1 contraction leading to a 76 cm × 13 cm smooth-wall working section which is 3 m in length. The maximum free-stream speed U_∞ is 30 m/sec and the free-stream turbulence level is approximately 0.1 percent. At $U_\infty = 7.3$ m/sec, the

boundary layer near the downstream end of the tunnel has a thickness of about 5 cm. A 90 cm × 90 cm tunnel, described by Hancock (1980), was also employed for a few checks on overall procedure and measurement technique.

5 Measurement conditions

Except for several measurement points at different freestream velocities, the measurements were made in a boundary layer with the following characteristics: freestream velocity $U_\infty = 7.3$ m/sec, boundary layer thickness $\delta_{99} = 46.6$ mm, displacement thickness $\delta_1 = 7.91$ mm, momentum thickness $\delta_2 = 5.63$ mm, shape factor $H = 1.41$, momentum thickness Reynolds number $Re_{\delta_2} = 2{,}620$, skin friction coefficient $C_f/2 = 0.00165$, friction velocity $U_\tau = 0.30$ m/sec, Clauser shape factor $G = 7.10$, and viscous length scale $\nu/U_\tau = 50$ μm.

6 Effects of spatial resolution on longitudinal velocity statistical properties

Results giving an indication of the effect of spatial averaging in the spanwise direction are presented in Fig. 2. Here normalized $\overline{u'^2}$ are given as measured using five sensors of 5 μm diameter and different lengths, and one subminiature sensor of 0.625 μm diameter and 160 μm length. For $d = 5$ μm, the profile having the highest $\overline{u'^2}$ was measured with a wire 0.8 mm long, $l/d = 160$ and $l^+ = 16$ (extent of spanwise averaging = 16 viscous lengths). Of the profiles presented, this one is also the closest to the "correct" subminiature result. When sensor lengths are greater ($l^+ = 34, 60$) or less ($l^+ = 7.0, 12$), magnitudes of $\overline{u'^2}$ are lower for $y^+ < 200$. In the latter two cases, the wires were so short that their length to diameter ratio was 200 or less, and frequency response was reduced as a result of conduction from the wires to the support stubs (see Ligrani & Bradshaw 1987). When $l^+ = 34$ and 60, magnitudes of total longitudinal energy are lower because signals from fluctuating motions having spanwise length-scales smaller than the sensor length are seriously attenuated. These four lowest profiles show significant differences from the subminiature result, which could be considered to be errors if such measurements were erroneously believed to include all the energy in the turbulence spectra. A closer look at Fig. 2 also shows that the character of individual profiles and amount of response reduction changes at different boundary layer locations depending on whether support-stub conduction or "eddy-averaging" is most affecting sensor response. Here, the mean profile was measured with the subminiature sensor and seems to be acceptably accurate down to $y^+ = 3-5$.

In order to determine how the longitudinal turbulence energy is affected by spatial averaging, the peak value of $\sqrt{\overline{u'^2}}/U_\infty$ (strictly, the value of $y^+ = 17 \pm 0.5$) was measured with sensors having different lengths.

Magnitudes of $\sqrt{\overline{u_m'^2}}$, the peak value of longitudinal turbulence intensity, are shown in Fig. 3 normalized with respect to the freestream velocity. These quantities are shown as they vary with normalized sensor length l^+ and diameter d^+. Each symbol represents a measurement obtained with one of 21 different sensors all at $\nu/U_\tau = 50$ μm,

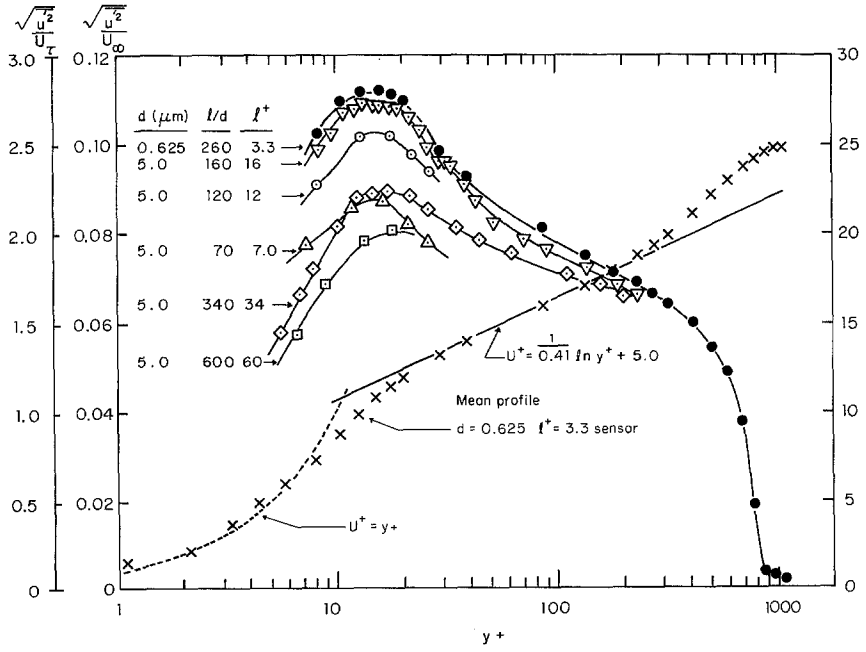

Fig. 2. Normalized longitudinal turbulence energy profiles measured using sensors having different spanwise extends and different diameters

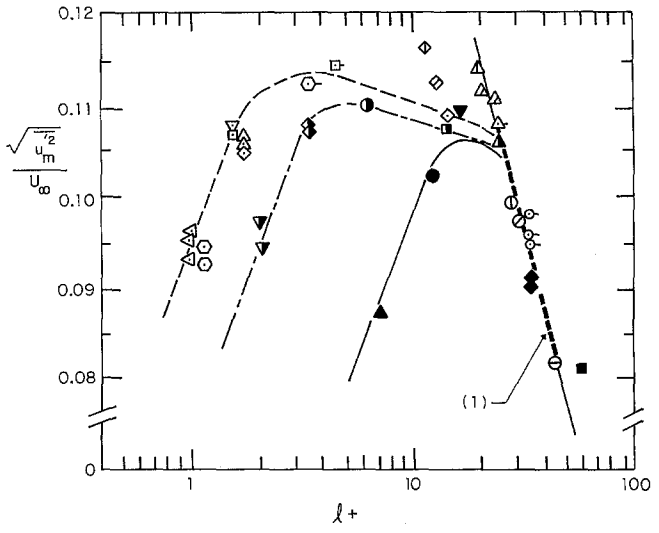

Results for varying viscous length: U_∞ (m/s)	ν/U_τ (μm)	d =0.625 m sensors l = 700 μm	l = 1200 μm	l = 1700 μm
5.71	62.4	◈	◬	◑
6.51	55.3	◈	◬	⊘
7.23	50.3	ALL OTHER SYMBOLS*		
9.90	37.9			⊖

*All other symbols show l^+ and d^+ dependence at U_∞ = 7.23 m/s, ν/U_τ = 50.3 μm, where each symbol represents measurements from a different sensor: open symbols, d=0.625 μm, d^+=0.012; half-open symbols, d = 1.25 μm, d^+=0.025; closed symbols, d = 5 μm, d^+=0.099.

Fig. 3. Dependence of normalized longitudinal turbulence energy on ratio of wire length to viscous length, and ratio of wire diameter to viscous length at $y^+ = 17$. ◇- ⊡- ◈- ◬- ⊙-, correspond to spectra in Fig. 10

with the exception of eight points obtained using $d =$ 0.625 μm sensors at viscous length scales different from 50 μm.

The shapes of the top and right hand portions of the $\nu/U_\infty = 50$ μm curves in Fig. 3 are a result of variations of the ratio of wire length to eddy size, represented by the abscissa l^+. On the right-hand side of the "plateaus", data points collapse on the same curve regardless of viscous length scale or non-dimensional wire diameter, d^+. The decrease of $\sqrt{\overline{u'^2}}/U_\infty$ with increasing non-dimensional sensing length l^+ is due to the greater amount of "eddy-averaging" which occurs as the spatial-resolution of sensors becomes less, and becomes rather rapid in the present flow when sensor length is greater than 1.0 mm, which corresponds to about 20 viscous length scales or $l/y > 1.1$. Such behavior results since hot-wire sensors act as spatial filters with a gradual low-pass cut-off which is dependent on sensor length. As a simple example, if the cut-off were abrupt at a length scale exactly equal to sensor length, then results on the right-hand side of Fig. 3 would indicate energy levels over different ranges of length scale: the energy existing between length scales l_1^+ and l_2^+ would then equal the difference between $\overline{u'^2}$ measured using two sensors having these respective non-dimensional lengths.

In the range $25 < l^+ < 45$, reductions of $\overline{u_m'^2}$ due to spatial averaging may be presented by the empirical equation

$$\frac{\sqrt{\overline{u_m'^2}}}{U_\infty} = \left(\frac{\sqrt{\overline{u_m'^2}}}{U_\infty}\right)_a \left(\frac{l^+}{25}\right)^{-0.45}. \tag{1}$$

This equation is strictly valid only at $y^+ = 17$, but may be a useful guide throughout the sublayer. It is valid only for wires with large enough l/d to avoid the end-conduction effects that produce the discrepancies on the left-hand side of Fig. 3.[a] It is shown in Fig. 3 using 0.108 for $\left(\sqrt{\overline{u_m'^2}}/U_\infty\right)_a$, the normalized turbulence intensity for $l^+ = 25$, while $\sqrt{\overline{u_m'^2}}/U_\infty$ represents results measured at other l^+.

When $2.5 < l^+ < 20$–25, $\sqrt{\overline{u_m'^2}}/U_\infty$ increases slightly as l^+ decreases at given d^+. Overall, $\sqrt{\overline{u_m'^2}}/U_\infty$ varies about ± 4 percent about the mean over this l^+ range. Maximum values are measured when $l^+ = 3.28$ and

[a] The left-hand portions of curves in Figs. 3 and 4 show decreasing $\sqrt{\overline{u'^2}}/U_\infty$ as l^+ decreases due to conduction from sensors to supports, which occurs when $l/d < 200$ (see Ligrani & Bradshaw 1987). Discussion which follows refers to the top and right-hand portions of curves in these figures, where $l/d > 200$.

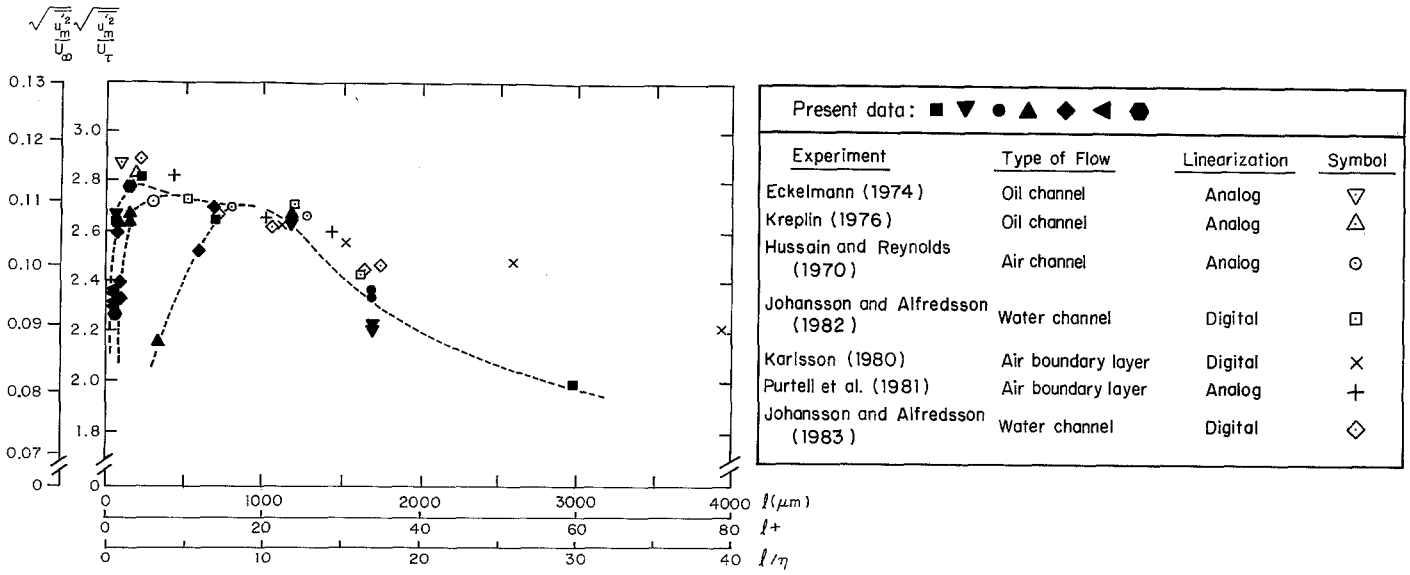

Fig. 4. Variation of normalized longitudinal turbulence energy with ratio of sensor length to viscous length scale for $y^+ \sim 17$. Solid symbols: present longitudinal velocity fluctuation data. Other symbols represent longitudinal velocity fluctuation data compiled by Johansson and Alfredsson (1983)

$l^+ = 4.47$, which gives some evidence that the highest (most accurate) $\overline{u'^2}$ are measured using the smallest possible sensor length with $l/d = 200-300$. For the minimum d^+ of the present study, 0.0124, l/d of 200 implies l^+ about 2.5.

The relatively small $\sqrt{\overline{u_m'^2}}$ changes for $l^+ < 20-25$ indicate that the minimum spanwise extent of energy-containing eddies is 20–25 viscous lengths at $y^+ = 17$.

Results in Fig. 3 are shown again in Fig. 4, where they are compared with results from other studies. In Fig. 4, all horizontal and vertical scales apply to the present data for $\nu/U_\infty = 50$ μm. Data from Hussain and Reynolds (1975), Eckelmann (1974), Kreplin and Eckelmann (1979), Karlsson (1980), Purtell et al. (1981), and Johansson and Alfredsson (1982, 1983) are also shown in $\sqrt{\overline{u'^2}}/U_\tau$ versus l^+ coordinates: the other ordinate and abscissa scales do not apply to these data. Other workers' data points represent the maximum longitudinal turbulence intensity measured at or near $y^+ = 17$. They are the same as given in Fig. 7 of Johansson and Alfredsson (1983) and were all obtained in boundary layer and channel flow using constant temperature anemometry. With the exception of Karlsson's (1980) data, these results show remarkable agreement with those of the present study. This verifies that many differences observed between different investigations are due to varying amounts of spanwise spatial filtering from sensors. The agreement also provides validation of $\sqrt{\overline{u'^2}}/U_\tau$ variations with l^+ shown, especially for $l^+ < 35$.

In Fig. 8 of their paper, Blackwelder and Haritonidis (1983) show bursting frequency data for $y^+ = 15$ in coordinates of $f^+ \equiv f\nu/U_\tau^2$ versus l^+, where f is the bursting frequency. They show that when plotted in logarithmic coordiantes, f^+ is "essentially constant for all sensors having a lengthscale less than $20\,\nu/U_\tau$". The bursting frequency data then show an abrupt drop in magnitude as the spanwise extent of sensors exceeds 20 viscous lengths. Non-dimensional bursting frequencies from the present study show a similar trend, lying 10–30% lower than the results of Blackwelder and Haritonidis (1983). Although the change in f^+ near $l^+ = 20-25$ is much greater than the change in intensity on a percentage basis, the same mechanism is probably responsible for both. Lee et al. (1974), Oldaker and Tiederman (1977), and Smith and Metzler (1983) give probability distributions of the non-dimensional spanwise streak spacing. These distributions showed continuously varying spacings with minimum values always approximately 20–25 viscous lengths. These results were obtained at y^+ values ranging from 1–30 over a range of Reynolds numbers. Thus, as Blackwelder and Haritonidis (1983) point out, "sensors having lengths greater than $20\,\nu/U_\tau$ would be larger than some of the streaks". Johansson and Alfredsson (1983) concluded that spatial averaging over spanwise distance less than about 30 viscous lengths occurs mostly in ejection-type motions rather than sweeps. Thus, variations of $\overline{u'^2}$ which occur as l^+ approaches 20–25 are probably from structures which developed from streaks and other streak-related events, in addition to the streaks themselves.

Our measurements of skewness factors and flatness factors with sensors spanning 3.3, 3.5, 4.4, and 8.6 viscous lengths are shown as functions of y^+ in Figs. 5 and 6, respectively. Within the scatter of the data in each figure, these profiles are the same. These data are compared with results from Johansson and Alfredsson (1983) for $l^+ = 14$ and $l^+ = 32$, showing agreement with the former, notably for $7 < y^+ < 30$ where the effects of spatial averaging are

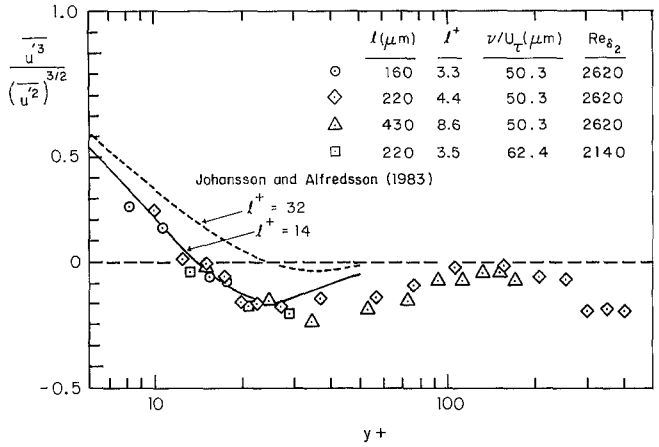

Fig. 5. Skewness factor distributions in near-wall boundary layer regions. $U_\infty = 7.23$ m/s, $\nu/U_\tau = 50.3$ μm, $Re_{\delta_2} = 2{,}620$ and $U_\infty = 5.77$ m/s, $\nu/U_\tau = 62.4$ μm, $Re_{\delta_2} = 2{,}140$ data

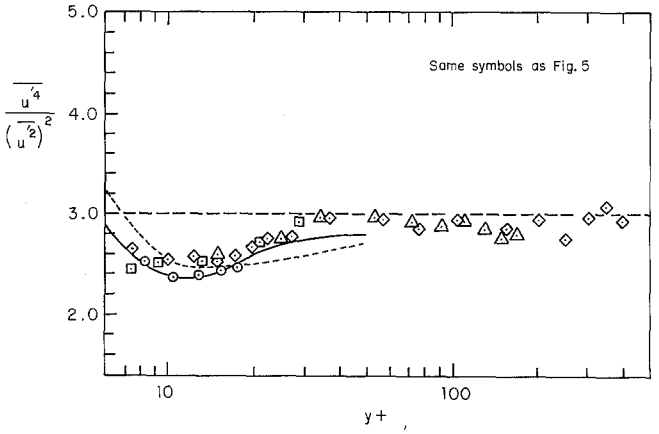

Fig. 6. Flatness factor distributions in near-wall boundary layer regions. $U_\infty = 7.23$ m/s, $\nu/U_\tau = 50.3$ μm, $Re_{\delta_2} = 2{,}620$ and $U_\infty = 5.77$ m/s, $\nu/U_\tau = 62.4$ μm, $Re_{\delta_2} = 2{,}140$ data

particularly significant. The difference between their profiles for $l^+ = 14$ and for $l^+ = 32$, suggests that a wire length of (very roughly) 20–25 viscous length scales may be a limiting value for measuring flatness factor and skewness factor as well as energy. Confirmation is provided in Fig. 7, where $\overline{u'^4}$ and $\overline{u'^4}/U_\tau^4$ are shown as determined from measurements at $y^+ = 17$ in our boundary layer with $Re_{\delta_2} = 2{,}620$, $U_\infty = 7.23$ m/sec. As for the $\sqrt{\overline{u_m'^2}}/U_\infty$ results, $\overline{u'^4}$ shows an abrupt drop in magnitude as l^+ becomes greater than 20–25. $\overline{u'^3}$ plotted in the same way did not show a consistent trend within data scatter, which is not surprising since $\overline{u'^3}$ is very nearly equal to zero at the peak in $\overline{u'^2}$ at $y^+ = 17$. Derksen and Azad (1983) show that flatness and skewness of u and du/dt do not have significant variation with wire length, but they do not indicate the range of l^+.

Probability density functions of the longitudinal velocity $P(u/U_\tau)$ at $y^+ = 17$ are shown in Fig. 8 for $l^+ = 3.3$, 24, and 34. Here, u denotes instantaneous longitudinal velocity, equal to $U + u'$. These density functions were estimated over abscissa intervals spaced $0.4\sqrt{\overline{u'^2}}$ apart from

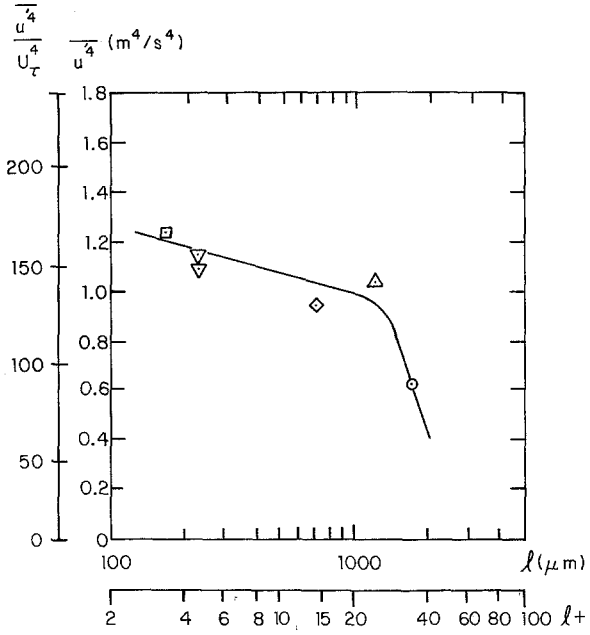

Fig. 7. Dependence of $\overline{u'^4}$ on sensor length at $y^+ = 17$ in turbulent boundary layer. $Re_{\delta_2} = 2{,}620$, $\nu/U_\tau = 50.3$ μm, $U_\infty = 7.2$ m/s

8 or more seconds of data sampled at 20 kHz. The $(u - U)/\sqrt{\overline{u'^2}}$ scale applies to all data, whereas the u (m/sec) and u/U_τ scales apply only to $l^+ = 3.3$ results. When $l^+ < 20$–25, most attenuation with sensor length occurs at velocities lower than the local mean velocity. However, for larger l^+, changes with sensor length become more significant, occurring at velocities as large as one standard deviation greater than the mean.

In Fig. 9, the variation of $\sqrt{\overline{u'^2}}/U_\infty$ and $\sqrt{\overline{u'^2}}/U_\tau$ with l^+ is shown at $y^+ = 8$, 12.5, 17, 20, 30, and 40. As one would expect, attenuation at given wire length becomes less severe as y increases and the energy-containing eddies become larger. The rapid drop in measured $\sqrt{\overline{u'^2}}$ near $l^+ = 20$–25, found in the detailed measurements at $y^+ = 17$, appears at all y^+ less than about 20: this suggests that the minimum spanwise scales of the energy-containing turbulence are roughly the same throughout the sublayer. For the three profiles nearest the wall, the $\sqrt{\overline{u'^2}}/U_\infty$ drop with l^+ becomes more abrupt as y^+ decreases. Such behavior is consistent with Smith and Metzler's (1983) probability-density histograms of spanwise streak spacing for $Re_{\delta_2} = 2{,}030$, described using log-normal distribution functions. These show a broadening of the streak distribution with increased distance from the wall, and, as y^+ decreases, more abrupt drops in probability magnitude as the ratio of streak spacing to viscous length decreases below 20–25.

7 Dissipation spectra and spatial resolution

If one assumes that the small scale turbulence is isotropic and that Taylor's "frozen-flow" approximation is valid,

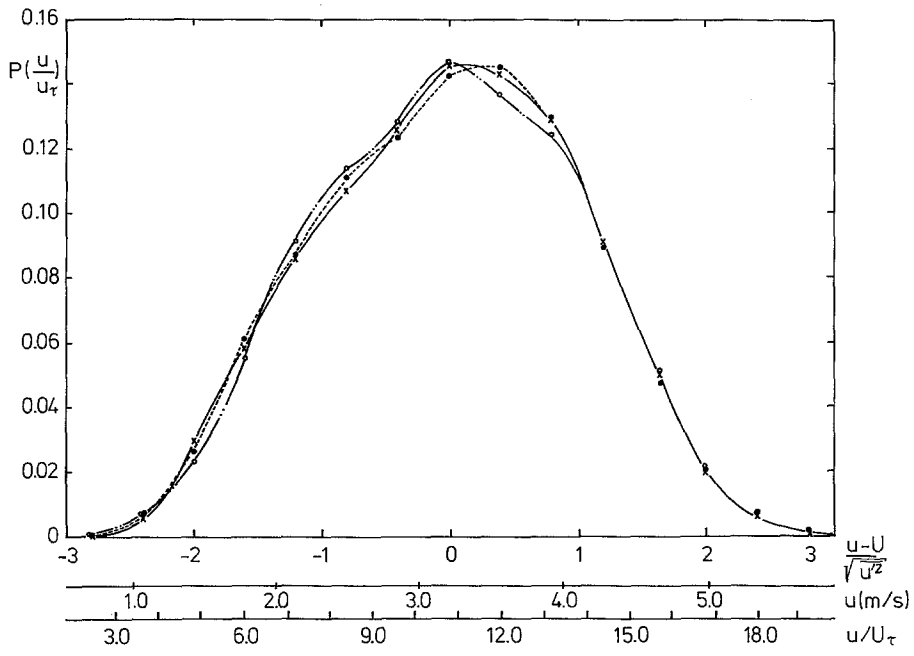

Fig. 8. Probability density functions of the longitudinal velocity at $y^+ = 17$ for different sensor lengths: —×— $l^+ = 3.3$, —●— $l^+ = 24.0$, —·—○— $l^+ = 34$

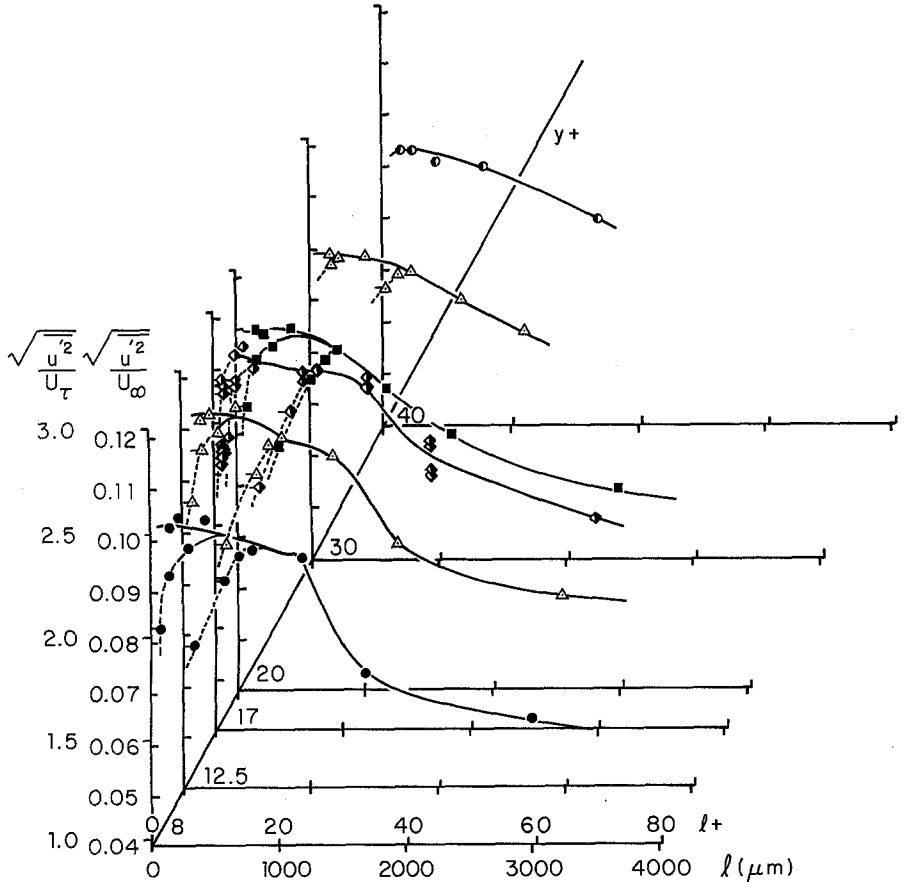

Fig. 9. Dependence of normalized longitudinal turbulence intensity on dimensional and non-dimensional wire length at different locations relative to the wall in boundary layer inner regions. ● $y^+ = 8$, △ $y^+ = 12.5$, ◆ $y^+ = 17$, ■ $y^+ = 20$, ▲ $y^+ = 30$, ◐ $y^+ = 40$. —— $l/d > 150$, – – – $l/d < 150$, $l/d < 150$ also for symbols with tick marks: -●-△-◆-■-▲-◐

then dissipation may be calculated using

$$\varepsilon = 15\,\nu \int_0^\infty k_1^2 f_u(k_1)\,dk_1 . \tag{2}$$

Here, $f_u(k_1)$ is the spectral energy per wavenumber such that

$$\int_0^\infty f_u(k_1)\,dk_1 = \overline{u'^2} . \tag{3}$$

k_1 is the one-dimensional wavenumber of longitudinal component of the three-dimensional wavenumber vector, estimated using $2\pi n/U$, where n is the frequency in Hz and U is the local mean velocity. The Kolmogorov length scale

$$\eta = (\nu^3/\varepsilon)^{1/4} \tag{4}$$

can then be obtained. Equations (2) and (4) give only very rough estimates of ε and η at $y^+ = 17$ because the turbulence is far from isotropic in the sublayer.

In order to show how the wavenumber portions of spectra vary with sensor length, dissipation spectra are given in Fig. 10, where $k_1^2 f_u(k_1)$ in cm/sec^2 is shown plotted versus k_1 in cm^{-1}. These spectra correspond to the $d^+ = 0.0124$ "open" data points in Fig. 3 with small "tick" marks on the symbols. Even though the measured $\sqrt{\overline{u'^2}}/U_\infty$ varies only slightly with l^+ for $l^+ < 20-25$ and $d^+ = 0.0124$, dissipation spectra show significant changes with sensor length. Because of spatial filtering, sensors slice off larger portions of the true spectrum, starting at the high wavenumber end, as l^+ increases: sensor lengths longer than 20–25 viscous lengthscales affect the energy containing portions of wavenumber spectra, whereas smaller length sensors do not. For l^+ near 20–25, spectra show wire-length dependence at frequencies as low as 40 Hz or $k_1 l = 0.15$ (Ligrani & Bradshaw 1987). This frequency is equivalent to streamwise wave lengths of about 100 mm or about 2,000 viscous lengths, a relatively large value consistent with the existence of near-wall streaky structures elongated in the longitudinal direction. For sensor lengths smaller than 20–25 viscous lengths, "eddy-averaging" continues to occur, but only in the dissipation range of wavenumbers which do not contain significant portions of the total longitudinal turbulence energy. This is evident from Fig. 10, where dissipation spectral peaks increase as sensor length decreases for $l^+ > 3.3$. The power in the dissipation spectra is insignificant at wavenumbers k_1 which are smaller than $1/\eta$. For our measurements conditions at $y^+ = 17$, this $k_1\eta = 1.0$ limit corresponds to $k_1 = 100$ cm^{-1} or $k_1 l = 1.6$ for our 160 μm wire.

Dissipation spectral variations with sensor length are further elucidated in Fig. 11, where η is shown, as determined from each spectrum using Eqs. (2) and (4). Here, the value of η used for abscissa normalization is denoted $\hat{\eta}$ and is equal to 100 μm – the best estimate for our flow condition. As $l/\hat{\eta}$ varies, η shows significant changes

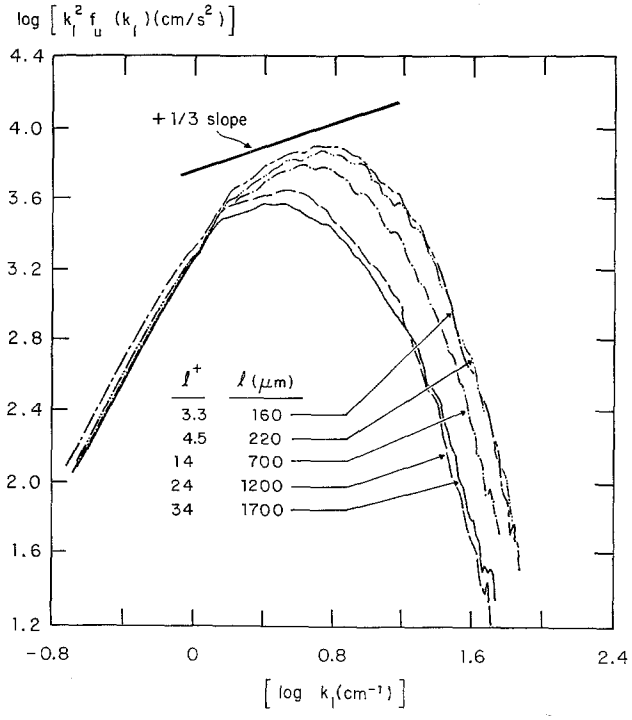

Fig. 10. Dissipation spectra of longitudinal velocity fluctuations as dependent on sensor length: $y^+ = 17$, $\eta = 100$ μm, $\nu/U_\tau = 50.3$ μm, $U_\infty = 7.2$ m/s, $Re_{\delta_2} = 2{,}620$. All sensors have 0.625 μm diameters. ⊙– ⊡– ◇– △– ⊙– are corresponding data points in Fig. 3

particularly as $l/\hat{\eta}$ becomes less than 12–14, which corresponds to l^+ less than 24–28. The rate of change of dissipation spectra decreases for $l/\hat{\eta} < 4$; however, it is not clear that they have stopped changing, due to the uncertainty of the measurements and some doubts concerning the spectrum from the 220 μm long sensor (see Ligrani & Bradshaw 1987). In Fig. 11, the arrow denotes Kolmogorov length scales estimated for locally-isotropic turbulence with equal rates of production and dissipation. Under these conditions,

$$\eta^+ = (\varkappa y^+)^{1/4} \tag{5}$$

where $\eta^+ = \eta U_\tau/\nu$ and $\varkappa = 0.41$. Magnitudes of η estimated using Eq. (5) are lower than estimated from dissipation spectra by about 20%, indicating that the spectra underestimate the dissipation. Note that η depends only on $\varepsilon^{-1/4}$ and is therefore not very sensitive to errors in ε.

8 Conclusions

Twenty-one different single-hot-wire sensors have been used in turbulent boundary layers developing over smooth, flat surfaces in order to determine the effects of spanwise spatial averaging on the statistical properties of the longitudinal velocity fluctuations. As the length (spanwise extent) of the sensors increases above 20–25 viscous lengths, the measured intensity, flatness factors, and

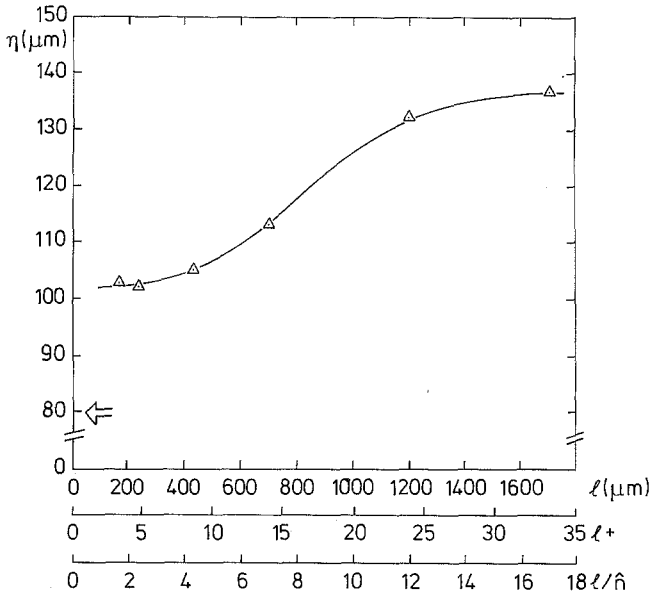

Fig. 11. Variation of Kolmogorov length scale with non-dimensional sensor length from estimates of dissipation determined from integrating spectra shown in Fig. 10. $\hat{\eta} = 100$ μm was used to normalize l on the abscissa

skewness factors decrease significantly and abruptly. This is most evident for $8 < y^+ < 17.5$, and the change becomes larger and more abrupt as the wall is approached. For $l^+ < 20-25$, the measured intensity changes less than 4%, increasing slightly as l^+ decreases, and flatness and skewness factor profiles are the same within data scatter. As well as defining the maximum sensor length acceptable for sublayer studies, these results show that comparatively few energy-containing motions have spanwise extends much less than 20–25 viscous length scales. This is consistent with probability-density histograms from other studies (e.g. Smith & Metzler 1983) which show minimum spanwise streak spacing to be about 25 viscous length scales.

At $y^+ = 17$, measured dissipation spectra show significant changes as l^+ varies from 14.0 to 3.3, which is equivalent to $l/\hat{\eta}$ variations from 7.0 to 1.6. This indicates the existence of significant energy in motions having wave lengths only a few times the Kolmogorov length scale η within these ranges. There is no positive evidence that measured spectra would be independent of wire length even for $l^+ < 3$, but overall intensity seems to vary slowly with l^+ for $l^+ < 20$.

The results also show significant effects of conduction to the supports for $l/d < 200$: the final conclusion is that adequately accurate results for the mean-square and higher moments of the longitudinal velocity fluctuations near the wall can be obtained if $l^+ \equiv U_\tau l/\nu < 20$ and $l/d > 200$, and such results are presented here.

Acknowledgements

The first author was supported by the Science and Engineering Research Council of Great Britain (SERC Reference GR/C/07346) in order to develop and qualify the sensors used in the investigation. The first part of the study of the effects of sensor spatial resolution began under support from this organization, and was later continued under the auspices of the Office of Naval Research (Grant No. N 00014-84-G-0117, NR 679-007). For the latter, Dr. R. E. Whitehead was the program manager. All measurements were made in the laboratories of the Department of Aeronautics, Imperical College, London.

References

Blackwelder, R. F.; Haritonidis, J. H. 1983: Scaling of the bursting frequency in turbulent boundary layers. J. Fluid Mech. 132, 87–103

Blackwelder, R. F.; Kaplan, R. E. 1976: On the wall-structure of the turbulent boundary layer. J. Fluid Mech. 76, 89–112

Bradshaw, P. 1967: The turbulence structure of equilibrium boundary layers. J. Fluid Mech. 29, 625–645

Bradshaw, P. 1972: Two-more wind tunnels driven by aerofoil-type centrifugal blowers. I.C. Aero. Report 72-10, April 1972, Imperial College, London, GB

Bremhorst, K. 1972: The effect of wire length and separation on X-array hot-wire anemometer measurements. IEEE Trans. Instrum. Meas. 21, 244–248

Collis, D. C.; Williams, M. J. 1959: Two-dimensional convection from heated wires at low Reynolds numbers. J. Fluid Mech. 6, 357–384

Corrsin, S.; Kovasznay, L. S. G. 1949: On the hot-wire length correction. Phys. Rev. 75, 1954

Derksen, R. W.; Azad R. S. 1983: An examination of hot-wire length corrections. Phys. Fluids 26, 1751–1754

Dryden, H. L.; Schubauer, G. B.; Mock, W. C.; Skramstad, H. K. 1937: Measurements of intensity and scale of wind-tunnel turbulence and their relation to the critical Reynolds number of spheres. NACA Technical Report 581

Eckelmann, H. 1974: The structure of the viscous sublayer and the adjacent region in a turbulent channel flow. J. Fluid Mech. 65, 439–459

Frenkiel, F. N. 1949: The influence of the length of a hot wire on the measurements of turbulence. Phys. Rev. 75, 1263–1264

Frenkiel, F. N. 1954: Effects of wire length in turbulence investigations with a hot-wire anemometer. Aeronaut. Q. 5, 1–24

Hancock, P. E. 1980: The effect of free-stream turbulence on turbulent boundary layers. Ph.D. Thesis, Department of Aeronautics, Imperial College, London, GB

Hinze, J. O. 1975: Turbulence. (2nd ed.) New York: McGraw-Hill

Hussain, A. K. M. F.; Reynolds, W. C. 1975: Measurements in fully developed turbulent channel flow. ASME Trans. J. Fluids Eng. 97, 568–578

Johansson, A. V.; Alfredsson, P. H. 1982: On the structure of turbulent channel flow. J. Fluid Mech. 122, 295–314

Johansson, A. V.; Alfredsson, P. H. 1983: Effects of imperfect spatial resolution on measurements of wall-bounded turbulent shear flows. J. Fluid Mech. 135, 409–421

Karlsson, R. 1980: Studies of skin friction in turbulent boundary layers on smooth and rough walls. Doctoral Thesis, Dept. of Applied Thermo and Fluid Dynamics, Chalmers Univ. Tesch., Gøteborg, Sweden

Kastrinakis, L.; Wallace, J. M.; Willmarth, W. W. 1975: Measurements of small scale streamwise vorticity in a turbulent channel flow. Bull. Am. Phys. Soc. 20, 1422

Kim, H. T.; Kline, S. J.; Reynolds, W. C. 1971: The production of turbulence near a smooth wall in a turbulent boundary layer. J. Fluid Mech. 50, 133–160

Klebanoff, P. S. 1954: Characteristics of turbulence in a boundary layer with zero pressure gradient. NACA Technical Note 3178

Kline, S. J.; Reynolds, W. C.; Schraub, F. A.; Runstalder, P. W. 1967: The structure of turbulent boundary layers. J. Fluid Mech. 30, 741–773

Kreplin, H.-P.; Eckelmann, H. 1979: Behavior of the three fluctuating velocity components in the wall region of a turbulent channel flow. Phys. Fluids 22, 1233–1239

Lee, M. K.; Eckelman, L. D.; Hanratty, T. J. 1974: Identification of turbulent wall eddies through the phase relation of the components of the fluctuating velocity gradient. J. Fluid Mech. 66, 17–33

Ligrani, P. M. 1984: Subminiature hot-wire sensor construction. Report NPS69-84-010, Department of Mechanical Engineering, Naval Postgraduate School, Monterey/CA, USA

Ligrani, P. M.; Bradshaw, P. 1987: Subminiature hot wire sensors: development and use. J. Phys. E. (in print)

Ligrani, P. M.; Moffat, R. J. 1986: Structure of transitionally rough and fully rough turbulent boundary layers. J. Fluid Mech. 162, 69–98

Oldaker, D. K.; Tiederman, W. G. 1977: Spatial structure of the viscous sublayer in drag-reducing channel flows. Phys. Fluids 20, 5133–5144

Pao, Y. 1965: Structure of turbulent velocity and scalar fields at large wavenumbers. Phys. Fluids 8, 1063–1075

Purtell, L. P.; Klebanoff, P. S.; Buckley, F. T. 1981: Turbulent boundary layer at low Reynolds number. Phys. Fluids 24, 802–811

Roberts, J. B. 1973: On the correction of hot wire turbulence measurements for spatial resolution errors. Aeronaut. J. 77, 406–412

Smith, C. R. 1984: A synthesized model of the near-wall behavior in turbulent boundary layers. In: Proceedings of Eighth Symposium on Turbulence (eds. Patterson, G. K.; Zakin, J. L.). Department of Chemical Engineering, University of Missouri at Rolla, USA

Smith, C. R.; Metzler, S. P. 1983: The characteristics of low-speed streaks in the near-wall region of a turbulent boundary layer. J. Fluid Mech. 129, 27–54

Smol'yakov, A. V.; Tkachenko, V. M. 1983: The measurement of turbulent fluctuations: An introduction to hot-wire anemometry and related transducers. (ed. Bradshaw, P.). Berlin, Heidelberg, New York: Springer-Verlag

Tennekes, H.; Lumley, J. L. 1972: A first course in turbulence. Boston: MIT Press

Uberoi, M. S.; Kovasznay, L. S. G. 1953: On mapping and measurement of randon fields. Q. Appl. Math. 10, 375–393

Willmarth, W. W.; Bogar, T. J. 1977: Survey and new measurements of turbulent structures near the wall. Phys. Fluids 20, S9–S21

Willmarth, W. W.; Sharma, L. K. 1984: Study of turbulent structure with hot wires smaller then the viscous length. J. Fluid Mech. 142, 121–149

Wyngaard, J. C. 1968: Measurement of small-scale turbulence structure with hot wires. J. Phys. E. 1, 1105–1108

Wyngaard, J. C. 1969: Spatial resolution of the vorticity meter and other hot-wire arrays. J. Phys. E. 2, 983–987

Wyngaard, J. C. 1971: Spatial resolution of a resistance wire temperatur sensor. Phys. Fluids 14, 2052–2054

Received September 4, 1986

Announcement

Fourth international symposium on applications of laser anemometry to fluid mechanics, July 11 – 14, 1988, Lisbon, Portugal

The symposium aims to present new methods of laser anemometry and new results of significance to fluid mechanics obtained by laser anemometry. It is intended that these results will improve present understanding of complex flows, both laminar and turbulent, and their implications for the solution of problems of fluid mechanics will be emphasized. Contributions to the theory and practice of laser anemometry will be presented where they facilitate new fluid-mechanic investigations.

Approximately 18 formal and Open Forum sessions are planned. Contributed papers are welcome in the following areas:

- jets, wakes, and mixing regions
- boundary layer flows
- separated flows
- reacting flows
- flows with imposed oscillations
- two phase flows
- particle sizing
- developments to optical and electronic instrumentation intended to improve accuracy and range of measurements
- whole field velocimetry

Paper selection will be based upon a reviewed abstract of not less than 500 words which should be typed double spaced and state the purpose, results and conclusions of the work with supporting figures as appropriate. Four copies of the abstract should be submitted to:

Prof. D. F. G. Durao, Dept. of Mechanical Engineering, Instituto Superior Técnico, Avenida Rovisco Pais, P-1096 Lisbon, Portugal.

Final date for receipt of abstracts:	December 16, 1987
Authors informed concerning acceptance:	February 26, 1988
Final date for receipt of camera-ready manuscripts:	May 13, 1988

All papers accepted for presentation will be incorporated in a Proceedings Volume which will be available at the time of the Symposium. It is intended that a bound volume will subsequently be published and will contain a selection of extended papers.